Atmospheric Environment 207 (2019) 63–74

Contents lists available at ScienceDirect

Atmospheric Environment

journal homepage: www.elsevier.com/locate/atmosenv

High resolution, extreme isotopic variability of precipitation nitrate

Lucy A. Rose*[,1], Zhongjie Yu, Daniel J. Bain, Emily M. Elliott

Department of Geology and Environmental Science, University of Pittsburgh, 4107 O'Hara St., Pittsburgh, PA, 15260, USA

ARTICLE INFO

Keywords:
Nitrate
Atmospheric deposition
$\delta^{15}N$
$\delta^{18}O$
$\Delta^{17}O$
NO_x

ABSTRACT

Deposition of atmospheric nitrate (NO_3^-) in precipitation can be an important source of reactive nitrogen (N) to ecosystems, particularly in regions with high nitrogen oxide (NO_x = nitric oxide (NO) + nitrogen dioxide (NO_2)) emissions. However, high resolution deposition data are lacking for most systems. We conducted hourly precipitation sampling across six growing season storms in a forested area historically subjected to some of the highest levels of chronic N deposition in the United States. To characterize the influence of electricity generating unit (EGU), vehicle, and biogenic NO_x emissions on NO_3^- deposition, we calculated the total NO_x emitted from these sources within a 100 km radius of air mass back trajectories determined for Fernow Experimental Forest (West Virginia, USA). We combined these emissions estimates with established ^{15}N isotope values for NO_x sources in a three end-member mixing model to predict source-based $\delta^{15}N$ values of deposition reaching the study site on an hourly basis. To evaluate the effect of NO_x oxidation pathways on measured $\delta^{15}N$-NO_3^- values, we compared observed hourly isotope values to a coupled $\delta^{15}N$ and $\Delta^{17}O$ array representing N isotope exchange between atmospheric oxidized N molecules. Within individual events, $\delta^{15}N$, $\delta^{18}O$, and $\Delta^{17}O$ values ranged by as much as 19.5‰, 28.9‰, and 13.8‰, respectively. This extreme short-term isotopic variability suggests a dynamic mix of NO_x sources, oxidation pathways, and fractionation processes contributing to HNO_3 formation. During every storm, precipitation $\delta^{15}N$-NO_3^- values were lower than those expected to result from predominant HNO_3 formation pathways or oxidation of estimated NO_x emissions along back trajectories, suggesting a systematic underestimation of NO_x contributions to atmospheric HNO_3 formation from isotopically depleted soil emissions. Together, these analyses represent the most comprehensive assessment to date relating high temporal resolution $\delta^{15}N$-NO_3^- observations to NO_x emission sources, oxidation chemistry, and isotopic fractionation effects. We present the first observations of extreme intra-storm $\delta^{15}N$, $\delta^{18}O$, and $\Delta^{17}O$ variability, emphasizing the need for improved constraints on soil NO_x emissions, forest canopy effects, and their role in atmospheric NO_3^- deposition and isotope dynamics in forests.

1. Introduction

Nitrogen deposition, in the form of wet and dry deposition of both oxidized and reduced N, is a source of nutrient loading to terrestrial and aquatic ecosystems, and chronically elevated rates of atmospheric N deposition have contributed to the degradation of ecosystem function worldwide (Driscoll et al., 2001; Grennfelt and Hultberg, 1986; Vitousek et al., 1997; Warby et al., 2009). Despite substantial reductions in NO_x emission rates across the U.S. in recent decades (De Gouw et al., 2014; Kim et al., 2006)— particularly from stationary emission sources such as electricity-generating units (EGUs)— oxidized forms of N still represent the dominant form of N deposition in the eastern U.S. (Schwede et al., 2018; Sun et al., 2016). Additional anthropogenic sources of atmospheric N include vehicles and fertilizer emissions, while lightning and biogenic soil emissions serve as natural sources of NO_x in the atmosphere.

Atmospheric NO_3^- is formed via complex cycling of nitrogen oxides (NO_x = nitric oxide (NO) + nitrogen dioxide (NO_2)) emitted from anthropogenic and natural sources. Once emitted, NO_x cycles between NO and NO_2 via the oxidation of NO by O_3 (Reaction 1) or peroxy radicals (HO_2 and RO_2) (Reaction 2) to form NO_2 and the daytime photolysis of NO_2 back to NO (Reaction 3) (Fig. 1). This interaction between NO and NO_2 occurs so rapidly under normal atmospheric conditions that a photochemical stationary state of NO_x is established within a few minutes during the day (Vicars et al., 2013).

$$NO + O_3 \rightarrow NO_2 + O_2 \quad \text{Reaction (1)}$$

$$NO + RO_2(or\ HO_2) \rightarrow NO_2 + RO(or\ OH) \quad \text{Reaction (2)}$$

* Corresponding author.
E-mail address: larose@umn.edu (L.A. Rose).
[1] Current address: Department of Forest Resources, University of Minnesota Twin Cities, 1530 Cleveland Ave. N., Saint Paul, MN 55108, USA.

https://doi.org/10.1016/j.atmosenv.2019.03.012
Received 6 December 2018; Received in revised form 7 March 2019; Accepted 11 March 2019
Available online 18 March 2019

$NO_2 + h\nu \rightarrow NO + O(^3P)$ Reaction (3)

$NO_2 + OH \rightarrow HNO_3$ Reaction (4)

$NO_2 + O_3 \rightarrow NO_3 + O_2$ Reaction (5)

$NO_2 + NO_3 \overset{M}{\leftrightarrow} N_2O_5$ Reaction (6)

$N_2O_5 + H_2O \overset{aerosol}{\rightarrow} 2HNO_{3(aq)}$ Reaction (7)

$NO_3 + RH \rightarrow HNO_3 + R$ Reaction (8)

NO_2 is removed from the atmosphere through oxidation and dry deposition to surfaces. During the daytime, NO_2 is oxidized by the hydroxyl radical (OH), forming HNO_3 (Reaction 4) (hereafter, referred to as the HNO_3(1) pathway). When the photochemical production of OH ceases during the nighttime, NO_2 is primarily oxidized by O_3 to produce the nitrate radical (NO_3) (Reaction 5), which exists at thermal equilibrium with NO_2 and dinitrogen pentoxide (N_2O_5) (Reaction 6). Subsequent heterogeneous hydrolysis of N_2O_5 on the surface of aerosol particles forms HNO_3 (Reaction 7) (hereafter, referred to as the HNO_3(2) pathway). Nighttime HNO_3 may also form through hydrogen abstraction from hydrocarbons (RH) by NO_3 (Reaction 8) (hereafter, referred to as the HNO_3(3) pathway). Due to the different HNO_3 formation pathways, the lifetime of NO_x against conversion to atmospheric NO_3^- in the boundary layer varies from a few hours (mid-to-high latitudes in summer, primarily via the OH pathway) to ~3 days (high latitudes in winter, primarily via the N_2O_5 pathway) (Levy et al., 1999), whereas the lifetime of atmospheric NO_3^-, mainly controlled by dry and wet deposition, is on the order of days to weeks (Finlayson-Pitts and Pitts Jr, 1999).

Being the product of the reactions among NO_x, O_3, and free radicals, atmospheric NO_3^- is well-suited to probe sources and processes driving the atmospheric NO_x cycle, especially through its stable isotope composition (Elliott et al., 2019, 2009; 2007; Felix et al., 2015; Felix and Elliott, 2013; Hastings et al., 2003; Heaton, 1990; Walters et al., 2018). In particular, given the finding that the isotopic compositions of major NO_x sources are relatively distinct, the N isotopic composition (denoted as $\delta^{15}N$) of atmospheric NO_3^- has great potential for characterizing and quantifying NO_x source contributions to the atmospheric NO_3^- pool. For example, $\delta^{15}N\text{-}NO_x$ values for EGUs range from +10.5‰ to +19.8‰ and are dependent on emission controls employed (selective catalytic reduction, selective non-catalytic reduction, low NO_x burners) (Felix et al., 2012). In comparison, $\delta^{15}N\text{-}NO_x$ values for vehicle sources range from −19.1‰ to +10.0‰, with the lowest isotope values and highest NO_x concentrations associated with cold engine conditions (Ammann et al., 1999; Felix and Elliott, 2014; Miller et al., 2017; Redling et al., 2013; Walters et al., 2015). $\delta^{15}N\text{-}NO_x$ of biogenic soil emissions has much lower values than those reported for fossil fuel NO_x sources, ranging from −59.8‰ to −19.9‰ (Felix and Elliott, 2014, 2013; Li and Wang, 2008; Yu and Elliott, 2017).

$\delta^{15}N$ of atmospheric NO_3^- also carries valuable information about the chemical processes driving the conversion of NO_x to atmospheric NO_3^- and their associated kinetic and equilibrium isotope effects. For example, previous work suggests that isotopic exchange between NO and NO_2 might alter $\delta^{15}N\text{-}NO_2$ values relative to $\delta^{15}N\text{-}NO_x$ (Freyer et al., 1993; Walters et al., 2016), which may then propagate to the $\delta^{15}N$ value of atmospheric NO_3^- (Savarino et al., 2013) (Fig. 1). Moreover, N isotope exchange processes involving NO_2, NO_3, and N_2O_5, the precursors in the three HNO_3 formation pathways (Fig. 1), have been recently investigated by Walters and Michalski (2015) and Walters et al. (2016), lending both theoretical and experimental support to the importance of these N isotope effects on $\delta^{15}N$ values of atmospheric NO_3^-. Based on these calculations, $\delta^{15}N\text{-}NO_3$ and $\delta^{15}N\text{-}N_2O_5$ are significantly lower and higher than $\delta^{15}N\text{-}NO_2$, respectively, under isotopic equilibrium conditions, suggesting that atmospheric NO_3^- produced from the three formation pathways is potentially distinguishable by its $\delta^{15}N$ signature (Walters and Michalski, 2015). However, while the sensitivity of $\delta^{15}N\text{-}NO_3^-$ to atmospheric oxidation reactions may be useful in elucidating the transformation of NO_x to HNO_3, it may complicate the use of $\delta^{15}N\text{-}NO_3^-$ in source partitioning of NO_x emissions. Therefore, to fully understand the mechanisms underlying $\delta^{15}N\text{-}NO_3^-$ and its spatiotemporal variability, a more comprehensive assessment that relates $\delta^{15}N\text{-}NO_3^-$ to both NO_x emission sources and chemistry effects is needed.

Importantly, oxygen isotopes ($\delta^{18}O$ and $\delta^{17}O$) of atmospheric NO_3^- can be used as an independent constraint on the oxidation pathways that control NO_x conversion to NO_3^- (Alexander et al., 2009; Hastings et al., 2003; Michalski et al., 2003). The distinctive ^{17}O-excess ($\Delta^{17}O$, defined as $\Delta^{17}O = \delta^{17}O - 0.52 \times \delta^{18}O$ in this study (Thiemens, 2006)) of atmospheric NO_3^- is a particularly useful isotopic fingerprint of NO_x transformations (Alexander et al., 2009; Michalski et al., 2014; Morin et al., 2009; Savarino et al., 2007; Vicars et al., 2013). The unique power of $\Delta^{17}O\text{-}NO_3^-$ stems from mass-independent fractionation during O_3 formation in the atmosphere, which results in an excess of ^{17}O over what is expected based on the abundance of ^{18}O in atmospheric O_3 (Thiemens, 2006). This $\Delta^{17}O$ signature of O_3 is transferred to NO_x during oxidation reactions, enabling the $\Delta^{17}O$ signature of atmospheric NO_3^- to serve as a marker of the influence of O_3 in its chemical formation (Michalski et al., 2003; Alexander et al., 2009; Morin et al., 2011). For example, nighttime reactions involving NO_3 and N_2O_5 lead to the formation of atmospheric NO_3^- with a relatively high $\Delta^{17}O$ inherited from O_3; conversely, the daytime production of NO_3^- leads to a lesser $\Delta^{17}O$ transfer as the photochemically produced radicals (OH, HO_2, RO_2) involved in the NO_x cycle possess negligible ^{17}O-excess (Michalski et al., 2003; Alexander et al., 2009; Morin et al., 2011). This disproportionality in $\Delta^{17}O$ transfer provides a unique approach for tracing atmospheric NO_3^- formation pathways, potentially filling some of the gaps in our understanding of N isotope fractionations during NO_x oxidation to HNO_3 (Fig. 1). However, few studies to date have coupled $\Delta^{17}O$ with $\delta^{15}N$ of atmospheric NO_3^- to examine the sources and processes driving the NO_x cycle and formation of atmospheric NO_3^-.

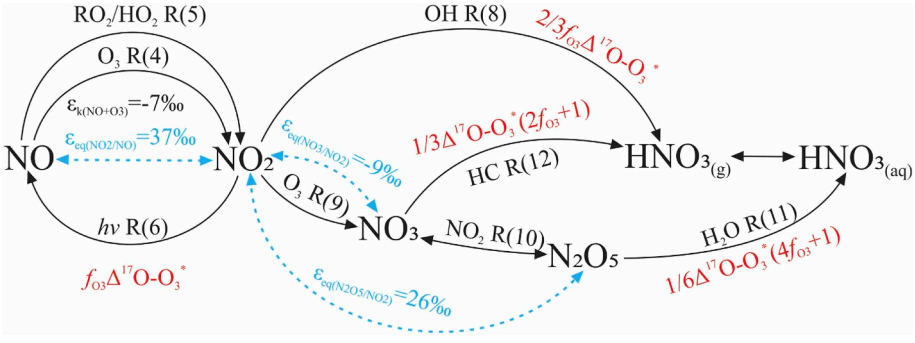

Fig. 1. Chemistry leading to formation of atmospheric nitrate (black text and arrows) and corresponding N isotope exchange equilibrium (blue arrows and text) and $\Delta^{17}O$ transfer from O_3 to nitrate (red text). (For interpretation of the references to colour in this figure legend, the reader is referred to the Web version of this article.)

While several previous studies have characterized NO_x emission and NO_3^- deposition dynamics on weekly, monthly, seasonal, annual, and longer time scales using $\delta^{15}N$ and $\delta^{18}O$ of atmospheric NO_3^- (Elliott et al., 2009, 2007; Felix and Elliott, 2014, 2013; Freyer, 1991; Hastings et al., 2003; Proemse et al., 2012; Redling et al., 2013), much less attention has focused on these dynamics at short time scales (e.g., diurnally and during individual storm events). Historically, this was likely due to sample mass requirements for isotopic analysis using combustion of silver nitrate (Kendall et al., 2007). For example, using this older method, Buda and DeWalle (2009) reported significant intra-storm variability in the $\delta^{15}N$ and $\delta^{18}O$ of NO_3^- during six storms in central Pennsylvania. During these events, within-storm isotopic ranges of up to 8.8‰ and 30.0‰ were reported for $\delta^{15}N$ and $\delta^{18}O$, respectively. The large range of values was attributed to changing air mass back trajectories and atmospheric oxidation chemistry during storms. However, the variability in $\delta^{18}O$ values may also reflect analytical artifacts of the silver nitrate method used to analyze precipitation samples in the Buda and DeWalle (2009) study; this method is susceptible to sample contamination effects that yield abnormally low $\delta^{18}O$ values in the atmospheric endmember (Revesz and Böhlke, 2002). More recently, Felix et al. (2015) attributed the highly variable $\delta^{15}N$ and $\delta^{18}O$ of NO_3^- values observed in sequential rainfall samples collected during Hurricane Irene (26–27 August 2011) to variations in NO_x source contributions along air mass back trajectories during that extreme rainfall event.

In this study, we present the results of triple NO_3^- isotope ($\delta^{15}N$, $\delta^{18}O$, and $\Delta^{17}O$) analyses of sequential precipitation samples collected approximately hourly during six growing season storm events at Fernow Experimental Forest (West Virginia, USA). We combine analyses of $\delta^{15}N$, $\delta^{18}O$, and $\Delta^{17}O$ to explore possible factors contributing to the highly variable isotopic composition of hourly precipitation NO_3^- collected in a densely forested mountainous setting during six growing season rainfall events. We use triple NO_3^- isotopes to assess the influence of variable NO_x source contributions, atmospheric oxidation pathways, and fractionation processes during NO_x conversion to NO_3^- on the short-term isotopic variability of precipitation NO_3^-.

2. Methods

2.1. Study site

This study was conducted at the USDA Forest Service Fernow Experimental Forest near Parsons, West Virginia USA (39°05′ N, 79°40′ W, 733 m asl; Fig. 2). Fernow is located in the Allegheny Mountains portion of West Virginia, where the annual average precipitation of 1450 mm is evenly distributed throughout the year (Kochenderfer, 2007). Mean monthly temperatures at Fernow range from −18.0 °C in January to +20.6 °C in July (Kochenderfer, 2007). During 2010, NO_3^- comprised approximately 60% of total inorganic wet N deposition (NO_3^- + NH_4^+) at Fernow, and particulate N deposition (HNO_3 + NO_3^- + NH_4^+) as measured by the EPA Clean Air Status and Trends Network (CASTNET) was approximately 25% of total wet N deposition (AMEC Environment & Infrastructure, Inc. (AMEC)., 2012; National Atmospheric Deposition Program, 2011).

2.2. Sample collection

We collected a total of 51 hourly precipitation samples during six storms in July and September 2010 (Table 1). Samples were collected in a small clearing adjacent to forested experimental watersheds WS3, WS4, and WS5 (Fig. 2). Precipitation was collected using two rectangular plastic containers (total area = 0.48 m^2) arranged in series and angled slightly downslope, with a hole drilled into the downslope corner. Intercepted precipitation drained into a 1 L sample bottle positioned beneath the downslope container. The suction tube of an automated sequential sampler (Teledyne ISCO, Inc.) was secured to the bottom of the sample bottle and once per hour, the autosampler collected all accumulated precipitation. Immediately prior to each storm, the plastic containers, sample bottles, and all autosampler bottles were triple-rinsed with 18 MΩ water. On 16 September, the first precipitation sample was collected approximately four hours after rainfall onset. Due to low precipitation intensities at the beginning of the 11 and 26 September events, the first samples for these storms represent a composite of all precipitation since the onset of rainfall. All precipitation samples were processed at the U.S. Forest Service Timber and Watershed Laboratory in Parsons, WV within 24 h. Samples were vacuum-filtered through 0.22 µm polyethersulfone (PES) membrane filters to remove suspended solids and biological material. All samples were frozen within 24 h after collection and transported to the University of Pittsburgh where they remained frozen until further analysis.

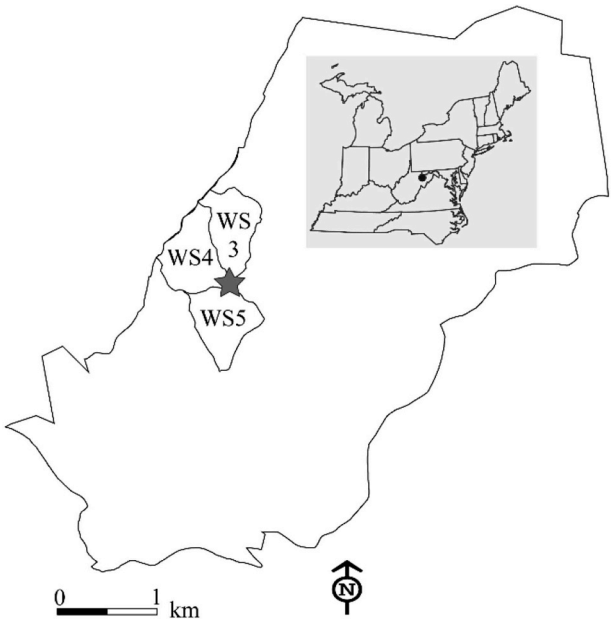

Fig. 2. Map of precipitation sampling site (denoted by star) and adjacent watersheds within the larger boundary of Fernow Experimental Forest (FEF). The black dot on the inset map shows the location of FEF in West Virginia, USA.

During periods of rainfall exceeding 2.1 mm h^{-1}, some precipitation may have overflowed the sample bottle. This threshold of rainfall intensity was exceeded for 14 of the 51 samples collected during the study. However, the possibility of some sample loss during the study does not alter our overall conclusions. For example, we observed substantial changes in isotopic composition between consecutive samples collected during periods of precipitation intensity well below the 2.1 mm h^{-1} threshold.

2.3. Isotopic analysis

Sample NO_2^- and NO_3^- concentrations were measured with ion chromatography (Dionex ICS-2000). Nitrite concentrations were lower than the instrument detection limit of 0.01 ppm in all samples except one collected during the 26 September event and another collected during the 30 September event. Nitrite was not removed from these samples prior to isotopic analysis; we observed no significant deviations in the patterns of $\delta^{18}O$-NO_3^- values during these events. For isotopic analysis, we used the bacterial denitrifier method, in which the denitrifying bacteria *Pseudomonas aureofaciens* was used to convert aqueous NO_3^- into gaseous N_2O which was then introduced into the mass spectrometer (Casciotti et al., 2002; Sigman et al., 2001). For $\Delta^{17}O$ analysis, the N_2O was thermally decomposed to N_2 and O_2 in a gold tube at 800 °C prior to isotopic analysis (Kaiser et al., 2007). Duplicate samples were analyzed for $\delta^{15}N$, $\delta^{18}O$, and $\Delta^{17}O$ of NO_3^- on an Isoprime Trace Gas and Gilson GX-271 autosampler coupled with an

Table 1
Characteristics of six storm events sampled at Fernow Experimental Forest during 2010.

Date	Rainfall in previous 30 days (mm)	Days since rain > 5 mm	Total rainfall (mm)	Storm duration (hr)	$[NO_3^-]$ and isotope ranges				Volume-weighted mean $[NO_3^-]$ and isotope values			
					$[NO_3^-]$ (mg L^{-1})	$\delta^{15}N$ (‰)	$\delta^{18}O$ (‰)	$\Delta^{17}O$ (‰)	$[NO_3^-]$ (mg L^{-1})	$\delta^{15}N$ (‰)	$\delta^{18}O$ (‰)	$\Delta^{17}O$ (‰)
9 July	61.7	14	17.7	8	0.16 to 2.77	−2.0 to +14.0	+62.0 to +82.0	+13.0 to +26.8	0.63	1.1	65.5	18.4
11 Sept	47.5	3	5.5	5	1.00 to 1.99	−4.3 to −2.0	+43.0 to +68.5	+12.8 to +23.4	1.51	−3.5	54.5	16.8
16 Sept	44.2	9	47.7	6	0.24 to 1.56	−4.5 to −1.7	+55.1 to +68.0	+11.2 to +20.4	0.50	−3.2	61.0	14.9
26 Sept	65.3	10	8.6	9	0.17 to 1.58	−12.4 to +4.9	+56.4 to +74.0	+19.6 to +29.0	0.65	−0.4	69.7	23.3
28 Sept	67.3	1	7.8	7	0.11 to 0.45	−6.6 to +1.3	+67.1 to +78.3	+22.1 to +30.6	0.19	−3.7	70.2	24.8
30 Sept	81.5	2	56.2	16	0.01 to 0.84	−6.5 to +13.0	+55.4 to +84.3	+17.4 to +26.5	0.11	2.3	64.1	22.5

Isoprime Continuous Flow Isotope Ratio Mass Spectrometer (CF-IRMS) at the Regional Stable Isotope Laboratory for Earth and Environmental Science at the University of Pittsburgh. Isotope values are reported in parts per thousand relative to the international N (atmospheric N_2) and O (Vienna Standard Mean Ocean Water) isotope standards as follows:

$$\delta^{15}N,\ \delta^{18}O,\ and\ \delta^{17}O(‰) = \left[\left(\frac{R_{sample}}{R_{standard}}\right) - 1\right] \times 1000 \quad (1)$$

where $R = {}^{15}N/{}^{14}N$, ${}^{18}O/{}^{16}O$, or ${}^{17}O/{}^{16}O$. The mass-independent oxygen isotope anomaly of NO_3^- ($\Delta^{17}O\text{-}NO_3^-$) is likewise reported in parts per thousand and calculated as (Michalski et al., 2003; Thiemens, 2006):

$$\Delta^{17}O(‰) = \delta^{17}O - 0.52 \times \delta^{18}O \quad (2)$$

Samples with low NO_3^- concentrations were pre-concentrated prior to bacterial conversion to N_2O. Pre-concentration was accomplished by determining the sample volume necessary to obtain a final concentration of 20 nmol (for $\delta^{15}N$ and $\delta^{18}O$ analysis) or 200 nmol (for $\Delta^{17}O$ analysis) in a 5 mL sample. Appropriate sample volumes were measured into 10% hydrochloric acid-washed Pyrex or Teflon beakers and placed in a drying oven at 60 °C until all liquid was evaporated. The interior of each beaker was then rinsed with 10 mL of 18 MΩ water to reconstitute duplicate samples to the appropriate concentration. Of the 51 precipitation samples collected during this sampling campaign, 8 samples required pre-concentration prior to $\delta^{15}N$ and $\delta^{18}O$ analysis; there was insufficient sample volume to pre-concentrate these samples for $\Delta^{17}O$ analysis. Due to the higher concentration requirements for $\Delta^{17}O$ analysis, 30 precipitation samples with sufficient sample volume required pre-concentration prior to $\Delta^{17}O$ analysis. We note that the heating temperature used in the pre-concentration step has the potential to evaporate ammonium nitrate (NH_4NO_3) that may have been present in precipitation samples. However, it is not likely that this affected the isotope values of pre-concentrated samples in this study based on several lines of evidence. First, sample peak heights during isotopic analysis were as expected, suggesting little or no NO_3^- loss during pre-concentration. Secondly, we followed the identical treatment principle (Carter and Fry, 2013) and the resulting isotope values of pre-concentrated isotopic standards were not significantly different than unconcentrated standards. Thirdly, the relatively acidic pH values (range: 4.61–4.99) in wet deposition and high sulfate (SO_4^{2-}) concentrations compared to reduced N concentrations in bulk wet and dry deposition samples collected weekly (or bi-weekly for ammonia (NH_3)) during the study period at an NADP and CASTNET sampling site 2 km from our study site (AMEC Environment & Infrastructure, Inc. (AMEC)., 2012; National Atmospheric Deposition Program, 2011) indicate that SO_4^{2-} and NO_3^- were likely not fully neutralized in precipitation. As NH_3 reacts preferentially with SO_4^{2-} (Behera and Sharma, 2010; Baek et al., 2004), NH_4NO_3 concentrations are assumed to be small when NH_3 concentrations are low relative to SO_4^{2-} (Seinfeld and Pandis, 2006). Thus, although the potential for NH_4NO_3 evaporation during sample pre-concentration exists, our results suggest that this mechanism was not a major factor influencing the isotope values of pre-concentrated samples, nor can it explain the extreme variability in isotope values across the entire dataset. More detailed discussion of wet and dry bulk deposition chemistry and the potential for NH_4NO_3 evaporation is presented in Table S1 and associated text in the Supplementary Information. Pre-concentrated samples were prepared for isotopic analysis following the bacterial denitrifier method as previously described. $\delta^{15}N$ and $\delta^{18}O$ values were corrected using international reference standards USGS-32, USGS-34, USGS-35, and IAEA-N3; USGS-34 and USGS-35 were used to correct $\Delta^{17}O$ values. These standards were also used to correct for linearity and instrument drift. Standard deviations for international reference standards were 0.2‰, 0.5‰, and 0.2‰ for $\delta^{15}N$, $\delta^{18}O$, and $\Delta^{17}O$, respectively.

In atmospheric NO_3^- samples with positive $\Delta^{17}O$ values,

contributions of $^{14}N^{14}N^{17}O$ to the *m/z* 45 signal can result in overestimation of $\delta^{15}N$ values by ~1–2‰ (Coplen et al., 2004). Corrections for mass-independent $^{14}N^{14}N^{17}O$ contributions to *m/z* 45 were evaluated following the relationship described in Coplen et al. (2004) where a 1‰ increase in $\delta^{15}N$ corresponds to an 18.8‰ increase in $\Delta^{17}O$. Corrected $\delta^{15}N$ values were 0.6‰–1.6‰ lower than uncorrected values, depending on the mass-independent contribution of $\Delta^{17}O$ in the sample. Because this correction factor is small relative to the range of precipitation $\delta^{15}N$ values observed and because we could not apply the correction to samples lacking $\Delta^{17}O$ data, the $\delta^{15}N$ values presented here do not include the mass-independent $\Delta^{17}O$ correction. However, given that the magnitude of $\delta^{15}N$ variability exceeds that of the correction by a factor of ~12, omission of the mass-independent $\Delta^{17}O$ correction does not significantly bias the patterns in $\delta^{15}N$ values and our interpretation of intra-storm isotope dynamics.

2.4. Quantifying hourly NO_x emission sources along back trajectories

To characterize the influence of EGU, vehicle, and biogenic NO_x emissions on NO_3^- deposition, we used the National Oceanographic and Atmospheric Administration (NOAA) Hybrid Single Particle Lagrangian Integrated Trajectory (HYSPLIT) model to calculate a 24-h back trajectory for each hourly precipitation sample collected during storm events (i.e., 51 back trajectories for 51 samples; Fig. 3 and Fig. S1). We chose a back trajectory duration of 24 h because it approximates the lifetime of NO_x in the near-surface troposphere (Alexander et al., 2009; Lamsal et al., 2010; Munger et al., 1998; Seinfeld and Pandis, 2006). Back trajectories were calculated at 500 m above ground level using the Eta Data Assimilation System (EDAS, 40 km resolution).

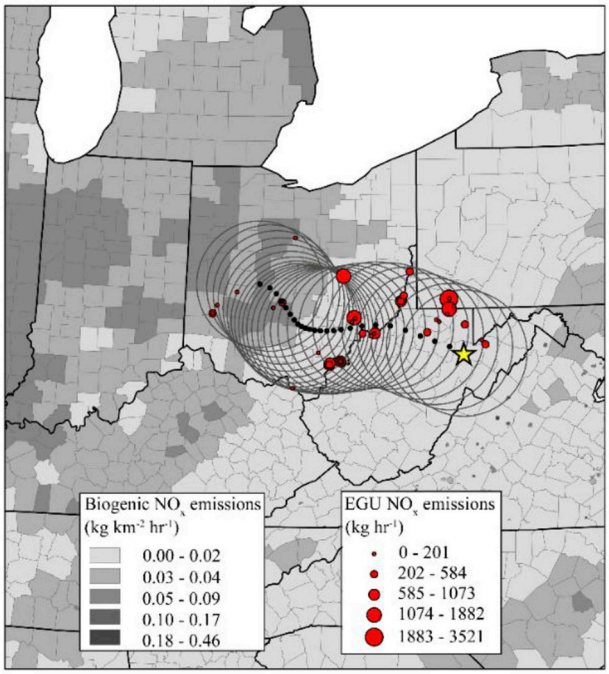

Fig. 3. Example 24-h back trajectory as determined by the NOAA HYSPLIT model. The starting point for all back trajectories was Fernow Experimental Forest (yellow star), and black dots represent hourly time steps along the modeled back trajectory. Larger gray circles show the 100 km buffer extent around each time step. County-level grayscale shading shows example biogenic NO_x emissions used to calculate biogenic source contributions along back trajectories; similar county-level data was also used for vehicle NO_x source quantification (not shown). Red circles show example EGU locations and emissions magnitude within 100 km buffer areas. (For interpretation of the references to colour in this figure legend, the reader is referred to the Web version of this article.)

For each hourly position along a 24-h air mass back trajectory, total NO_x emissions (tons per hour) within a 100 km radius were calculated for three dominant NO_x sources: EGUs, vehicles, and biogenic soil emissions. These sources were estimated to contribute 32, 60, and 6%, respectively, to the U.S. National Emission Inventory (NEI) in 2011 (U.S. Environmental Protection Agency, 2011). A radius of 100 km was chosen based on a prior evaluation of the relationship between bi-monthly $\delta^{15}N\text{-}NO_3^-$ values and EGU NO_x emissions summed within varying radial source areas of National Atmospheric Deposition Program monitoring sites across the Northeastern and Midwestern U.S. (Elliott et al., 2007). Total NO_x emissions for vehicle and biogenic sources were quantified at the county level as this was the finest spatial scale of available data. To calculate hourly biogenic and vehicle (on-road and off-road) NO_x emissions, we used modeled county-level estimates from the US EPA 2008 NEI (U.S. Environmental Protection Agency, 2008). We used estimates only for the months of July and September, assuming uniform hourly rates of biogenic and vehicle NO_x emissions county-wide. For EGUs, continuously measured, hourly NO_x emissions reported by individual units to the U.S. EPA are incorporated into the U.S. EPA Air Markets Program database (U.S. Environmental Protection Agency, 2015). We extracted hourly, unit level NO_x emissions for EGUs located within the 100 km buffer of individual hourly back trajectories for each of the six storm events. Only EGUs with NO_x emissions occurring at the time the projected air mass passed over the area were included in our calculations.

We further combined the estimated NO_x emissions from EGUs, vehicles, and soils with previously characterized $\delta^{15}N$ signatures of these three NO_x sources to estimate a representative $\delta^{15}N$ source signal for each hourly back trajectory. Based on a compilation of recent observations of $\delta^{15}N\text{-}NO_x$ source signatures (Elliott et al., 2019), we used 15 ± 5‰ (mean ± 1 standard deviation), −3 ± 5‰, and −36 ± 11‰ for NO_x emitted from EGUs, vehicles, and soils, respectively. Therefore, the $\delta^{15}N\text{-}NO_x$ source signature for each 24-h back trajectory was estimated by multiplying the mean $\delta^{15}N$ values of the three emission sources by their estimated fractional contributions.

2.5. Evaluation of NO_x oxidation pathways and fractionation effects

To evaluate NO_x oxidation pathways and their effects on measured $\delta^{15}N\text{-}NO_3^-$ values, we used a coupled $\delta^{15}N$ and $\Delta^{17}O$ array, similar to the one based on $\delta^{15}N$ and $\delta^{18}O$ of atmospheric HNO_3 proposed by Walters and Michalski (2016). This $\delta^{15}N\text{-}\Delta^{17}O$ array is based on the current understanding of N isotope exchange between atmospheric oxidized N molecules (Freyer, 1991; Walters and Michalski, 2016) and transfer of the mass-independent $\Delta^{17}O\text{-}O_3$ signal (Alexander et al., 2009; Michalski et al., 2003; Morin et al., 2011) during conversion of NO_x to atmospheric NO_3^- (Fig. 1).

During the daytime, NO_x exists as both NO and NO_2 due to emission of NO and NO_2 photolysis (Vicars et al., 2013). Therefore, daytime $\delta^{15}N\text{-}NO_2$ values will likely reflect a complex function of the $\delta^{15}N\text{-}NO_x$ and the N isotope partitioning between NO and NO_2 (Freyer et al., 1993; Walters and Michalski, 2015). Because the kinetic isotope effects associated with photochemical cycling of NO_x (Reactions 1, 2, and 3) and NO_2 oxidation by OH (Reaction 4) are currently unconstrained, we neglect these potential effects here and relate the $\delta^{15}N$ of atmospheric NO_3^- produced via the HNO_3(1) pathway to $\delta^{15}N\text{-}NO_x$ as the following:

$$\delta^{15}\text{N}-\text{HNO}_3(1) = \delta^{15}\text{N}-\text{NO}_2 = 1000\frac{[(^{15}\alpha_{NO2/NO} - 1)(1 - f_{NO2})]}{(1 - f_{NO2}) + (^{15}\alpha_{NO2/NO} f_{NO2})} + \delta^{15}\text{N}-\text{NO}_x \quad (3)$$

where f_{NO2} is the fraction of NO_2 relative to the total NO_x (i.e. $[NO_2]/[NO_x]$), and $^{15}\alpha_{NO2/NO}$ is the temperature-dependent N equilibrium isotopic fractionation factor for NO_2/NO. During the nighttime when most NO_x exists as NO_2 due to the absence of photochemical reactions, isotopic equilibrium between NO_2, NO_3, and N_2O_5 is likely to be

achieved mirroring its rapid chemical equilibrium (Reaction 6) (Freyer, 1991; Walters et al., 2016). Because the tropospheric concentrations of $[NO_2]$»$[NO_3]$»$[N_2O_5]$, the $\delta^{15}N$ values of N_2O_5 and NO_3 should reflect the equilibrium isotopic fractionation factors relative to NO_2 (i.e., $^{15}\alpha_{N2O5/NO2}$ and $^{15}\alpha_{NO3/NO2}$) (Walters and Michalski, 2015). Therefore, $\delta^{15}N$ of atmospheric NO_3^- produced from the HNO_3(2) and HNO_3(3) pathways can be related to $\delta^{15}N$-NO_x through $\delta^{15}N$-N_2O_5 and $\delta^{15}N$-NO_3 (Equations (4) and (5)), respectively (again neglecting currently unconstrained potential kinetic isotope fractionations associated with Reactions 7 and 8).

$$\delta^{15}\mathrm{N}-\mathrm{HNO_3}(2) = \delta^{15}\mathrm{N}-\mathrm{N_2O_5} = \delta^{15}\mathrm{N}-\mathrm{NO_2} + 1000(^{15}\alpha_{N2O5/NO2} - 1)$$
$$= 1000\left[\frac{(^{15}\alpha_{NO2/NO} - 1)(1 - f_{NO2})}{(1 - f_{NO2}) + (^{15}\alpha_{NO2/NO}\cdot f_{NO2})}\right] + \delta^{15}\mathrm{N}-\mathrm{NO_x}$$
$$+ 1000(^{15}\alpha_{N2O5/NO2} - 1) \quad (4)$$

$$\delta^{15}\mathrm{N}-\mathrm{HNO_3}(3) = \delta^{15}\mathrm{N}-\mathrm{NO_3} = \delta^{15}\mathrm{N}-\mathrm{NO_2} + 1000(^{15}\alpha_{NO3/NO2} - 1)$$
$$= 1000\left[\frac{(^{15}\alpha_{NO2/NO} - 1)(1 - f_{NO2})}{(1 - f_{NO2}) + (^{15}\alpha_{NO2/NO}\cdot f_{NO2})}\right] + \delta^{15}\mathrm{N}-\mathrm{NO_x}$$
$$+ 1000(^{15}\alpha_{NO3/NO2} - 1) \quad (5)$$

Calculation of $\Delta^{17}O$ of atmospheric NO_3^- produced from the three pathways is fundamentally based on the assumption that NO_x, O_3, and RO_2/HO_2 reach an isotopic equilibrium during both the daytime and nighttime (e.g. at dusk) (Alexander et al., 2009; Michalski et al., 2003). Accordingly, the $\Delta^{17}O$ value of NO_2 is determined at equilibrium by the relative production rate of NO_2 via reaction of NO with O_3 (Reaction 1) to the total NO_2 production (Reactions 1 and 2) (f_{O3}) and the mass-independent $\Delta^{17}O$ signal transferred from O_3 during Reaction 1 ($\Delta^{17}O$-O_3*):

$$\Delta^{17}\mathrm{O}-\mathrm{NO_2} = f_{O3}\cdot\Delta^{17}\mathrm{O}-\mathrm{O_3^*} \quad (6)$$

Importantly, $\Delta^{17}O$-O_3* is not equal to the bulk $\Delta^{17}O$ value of an O_3 molecule ($\Delta^{17}O$-O_3), but can be approximated as $1.5 \times \Delta^{17}O$-O_3 because of the isotopic asymmetry of O_3 combined with preferential transfer of the terminal oxygen atom from O_3 to NO during oxidation (Michalski and Bhattacharya, 2009). Therefore, the $\Delta^{17}O$ values of atmospheric NO_3^- produced from the three pathways can be calculated according to its involvement with O_3:

$$\Delta^{17}\mathrm{O}-\mathrm{HNO_3}(1) = \frac{2}{3}\cdot\Delta^{17}\mathrm{O}-\mathrm{NO_2} = \frac{2}{3}\cdot f_{O3}\cdot\Delta^{17}\mathrm{O}-\mathrm{O_3^*} \quad (7)$$

$$\Delta^{17}\mathrm{O}-\mathrm{HNO_3}(2) = \frac{5}{6}\cdot\Delta^{17}\mathrm{O}-\mathrm{N_2O_5} = \frac{1}{3}\cdot\Delta^{17}\mathrm{O}-\mathrm{NO_2} + \frac{1}{2}$$
$$\cdot\Delta^{17}\mathrm{O}-\mathrm{NO_3} = \frac{1}{6}\cdot\Delta^{17}\mathrm{O}-\mathrm{O_3^*}\cdot(4f_{O3} + 1) \quad (8)$$

$$\Delta^{17}\mathrm{O}-\mathrm{HNO_3}(3) = \Delta^{17}\mathrm{O}-\mathrm{NO_3} = \frac{2}{3}\cdot\Delta^{17}\mathrm{O}-\mathrm{NO_2} + \frac{1}{3}\cdot\Delta^{17}\mathrm{O}-\mathrm{O_3^*} = \frac{1}{3}$$
$$\cdot\Delta^{17}\mathrm{O}-\mathrm{O_3^*}\cdot(2f_{O3} + 1) \quad (9)$$

The $\Delta^{17}O$-HNO_3 values calculated according to Equations (7)–(9) implicitly assume that atmospheric OH, HO_2, and RO_2 have negligible $\Delta^{17}O$ signals (< 2‰) (Alexander et al., 2009; Michalski et al., 2003).

To parameterize the described $\delta^{15}N$-$\Delta^{17}O$ array for evaluation of the NO_x oxidation pathways and their effects on the measured $\delta^{15}N$-NO_3^- values, the estimated source $\delta^{15}N$-NO_x signatures for each hourly back trajectory (see above) were averaged for each precipitation event, and this event-specific $\delta^{15}N$-NO_x signal was used in Equations (3)–(5) to estimate the $\delta^{15}N$ values of atmospheric NO_3^- produced from the three pathways. It is further assumed that the daytime (Equation (3)) and nighttime (Equations (4) and (5)) f_{NO2} values range from 0.7 to 1 and 0.85 to 1, respectively, broadly consistent with observations conducted in the midwestern and northeastern United States (e.g., Buda and DeWalle, 2009; Walters et al., 2018). To estimate the $\Delta^{17}O$-HNO_3 values for the three pathways, the daytime (Equation (7)) and nighttime (Equations (8) and (9)) f_{O3} values were set to range between 0.2 to 1 and 0.9 to 1, respectively, consistent with the results of a global $\Delta^{17}O$-NO_3^- transport model (Alexander et al., 2009). We used a range of $\Delta^{17}O$-O_3 values, from 25 to 35‰ (corresponding to $\Delta^{17}O$-O_3* ranging from 37.5 to 52.5‰), generally found in the literature (Morin et al., 2011), for calculation of the $\Delta^{17}O$-NO_3^- endmembers. Given the above parameterization, Fig. 4 illustrates the possible ranges of $\delta^{15}N$ and $\Delta^{17}O$ values of HNO_3 produced from the three pathways, assuming a $\delta^{15}N$-NO_x signature of 12 ± 5‰, typical of locations dominated by EGU NO_x emissions.

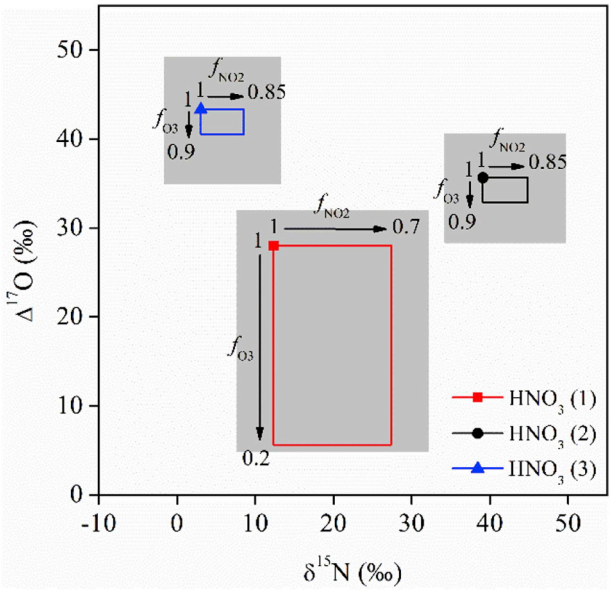

Fig. 4. Predicted $\delta^{15}N$-$\Delta^{17}O$ compositions for the three major HNO_3 production pathways based on N isotope exchange and transfer of the mass-independent $\Delta^{17}O$ signal during NO_x oxidation to HNO_3. The dots and lines denote the predicted $\delta^{15}N$-$\Delta^{17}O$ compositions of HNO_3 as a function of f_{NO2} and f_{O3} by assuming a $\delta^{15}N$-NO_x = 12‰ and a $\Delta^{17}O$-O_3 = 30‰. The gray shaded areas denote the possible ranges of $\delta^{15}N$-$\Delta^{17}O$ compositions of HNO_3 that account for assigned variations in $\delta^{15}N$-NO_x (7–17‰) and $\Delta^{17}O$-O_3 (25–35‰).

3. Results

3.1. Storm event 24-hour back trajectories

EGUs were the largest source of NO_x along 24-h air mass back trajectories for all rainfall events (Table S2). Integrated over each 24-h back trajectory, EGU NO_x accounted for 69–98% of total NO_x emissions, while vehicle and biogenic emissions comprised 1–30% and 0.2–2% of total NO_x emissions, respectively. Given that EGUs were consistently the dominant NO_x source, predicted $\delta^{15}N$-NO_x values closely resembled that of an EGU NO_x source signature, ranging from 11‰ to 14‰, with little temporal variation within each precipitation event (Fig. S2).

3.2. Precipitation nitrate concentrations

Across all storms, precipitation NO_3^- concentrations ranged from 0.01 to 2.77 mg L^{-1} (Table 1, Fig. 5). Storms differed in duration and pattern of precipitation input (Fig. 5), including short, intense downpours (16 and 30 September) and moderate, steady rainfall (11 and 26 September), but precipitation intensity measured at the study site was

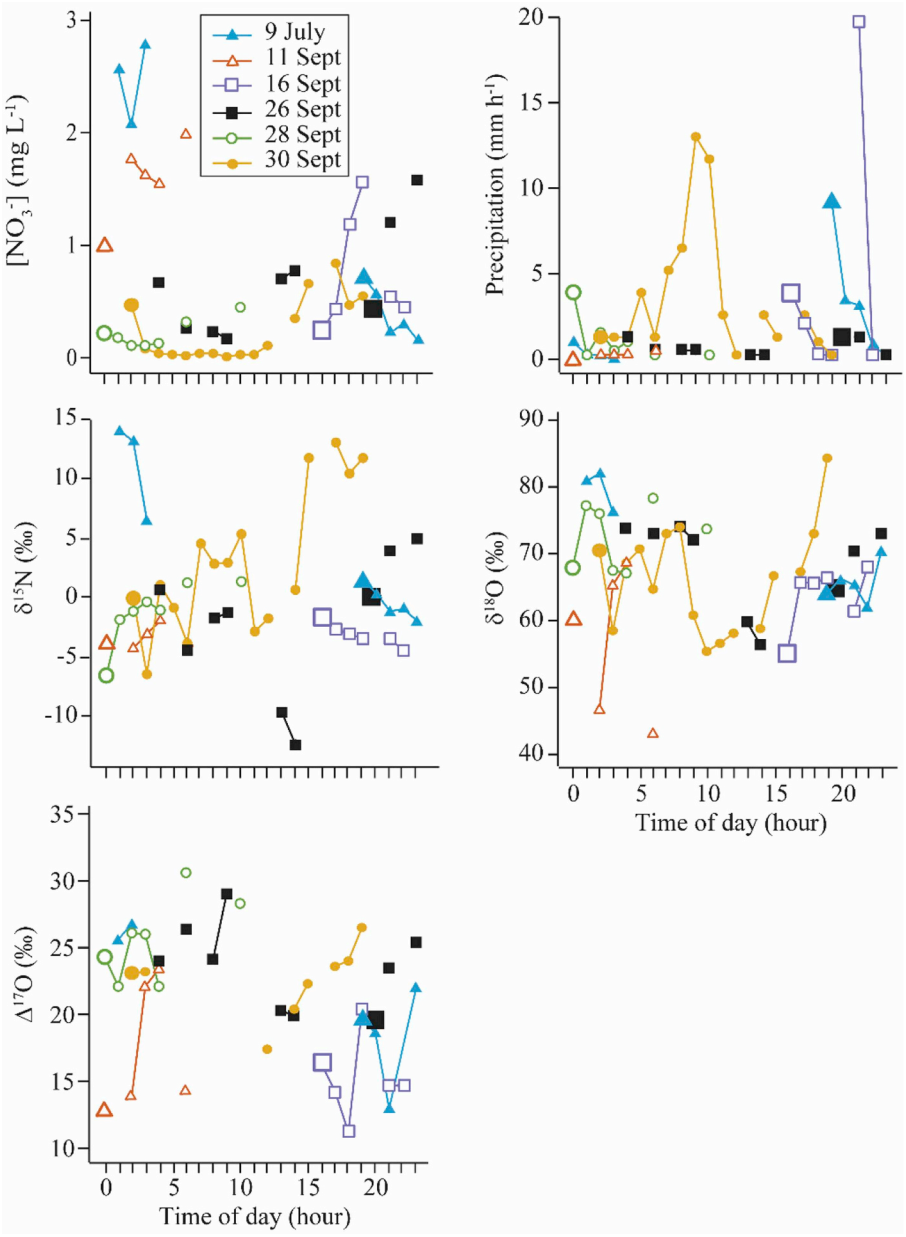

Fig. 5. Intra-storm variation in nitrate concentration, precipitation intensity, $\delta^{15}N$, $\delta^{18}O$, and $\Delta^{17}O$ of nitrate during six storms at Fernow Experimental Forest. The enlarged symbol in each series denotes the first sample collected during a storm; note that the 9 July and 26 Sept storms began in the evening and ended on the following day.

not correlated with NO_3^- concentration. Nitrate concentrations did decrease sharply during periods of high intensity precipitation on 16 September and 30 September, although the correlation between these variables was not statistically significant during either storm ($p > 0.1$ on both dates).

3.3. Triple isotopes of precipitation nitrate

The range of $\delta^{15}N\text{-}NO_3^-$ values across all precipitation events was −12.4 to +14.0‰ (Table 1), with large intra-storm variations in $\delta^{15}N$ values during some events (Fig. 5). For example, $\delta^{15}N$ values increased by nearly 16‰ over two hours on 9 July and by 12‰ over three hours on 30 Sept (Fig. 5). The temporal patterns in $\delta^{15}N$ also differed among storms. On 9 July and 26 September, values were low at the beginning of the storm, increased during the middle, then decreased toward the end. Conversely, $\delta^{15}N$ values during the 30 September event were initially high, but decreased sharply within a few hours, and then increased again shortly thereafter. $\delta^{15}N$ values during the 11 and 16 September events showed only minor intra-storm variability. Compared to the predicted $\delta^{15}N\text{-}NO_x$ source signatures, the measured $\delta^{15}N$ values in precipitation NO_3^- were lower for nearly every sample (Fig. S2). While some of the measured $\delta^{15}N\text{-}NO_3^-$ values were close to the predicted $\delta^{15}N\text{-}NO_x$ source signatures on 9 July, 26 September, and 30 September, a relatively consistent offset of about 14‰ between the measured $\delta^{15}N\text{-}NO_3^-$ and the predicted $\delta^{15}N\text{-}NO_x$ was observed on 11 September, 16 September, and 28 September (Fig. S2). Hourly $\delta^{15}N$ values showed significant positive relationships with total EGU NO_x emissions during the 9 July ($R^2 = 0.67$, $p = 0.01$), 16 September ($R^2 = 0.67$, $p = 0.04$), and 30 September ($R^2 = 0.47$, $p = 0.003$) storms, whereas $\delta^{15}N$ values were not significantly related to total biogenic or vehicle NO_x emissions during any storm.

Across all storms, $\delta^{18}O\text{-}NO_3^-$ values ranged from +43.0‰ to +84.3‰ (Table 1). As with $\delta^{15}N\text{-}NO_3^-$, intra-storm $\delta^{18}O\text{-}NO_3^-$ values were highly variable and storms showed differing temporal patterns in

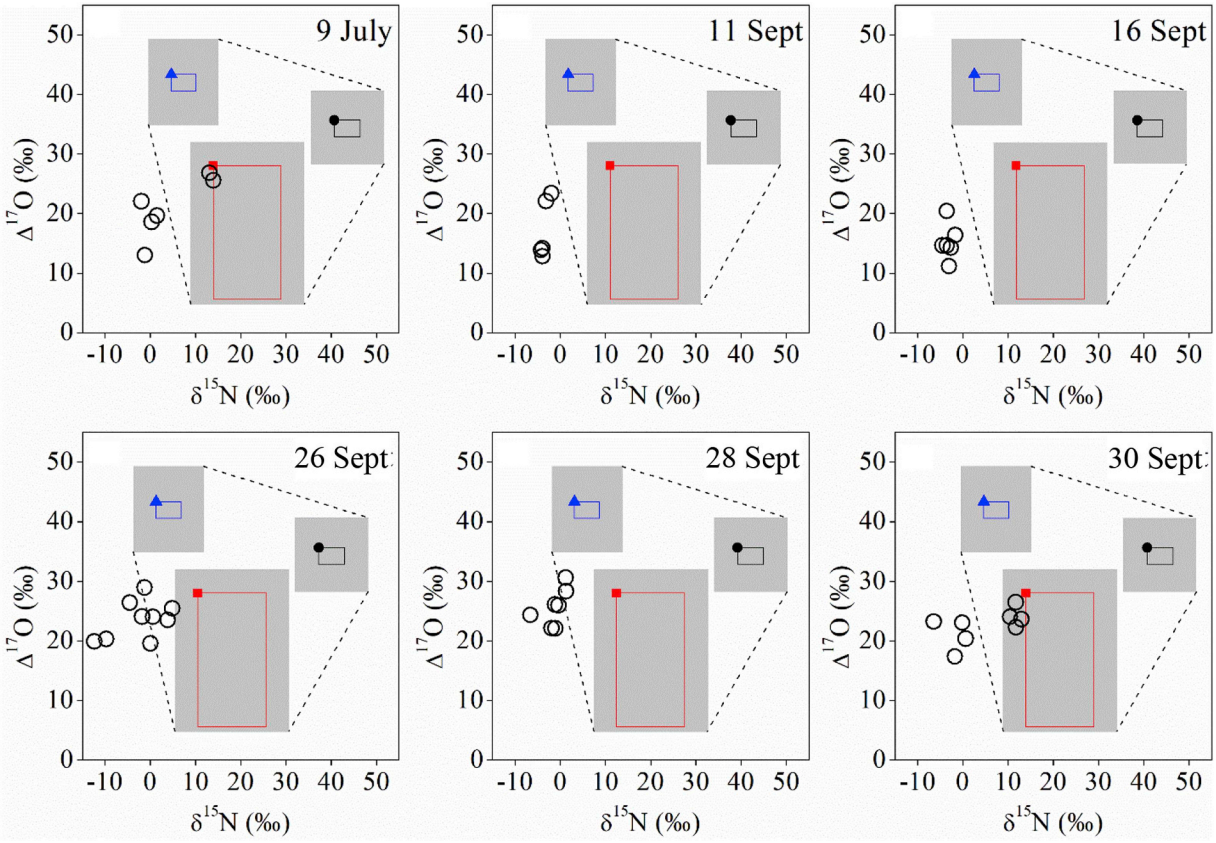

Fig. 6. The measured $\delta^{15}N\text{-}NO_3^-$ and $\Delta^{17}O\text{-}NO_3^-$ values (open circles) for each of the six storm events compared to the predicted $\delta^{15}N\text{-}\Delta^{17}O$ compositions for the three major HNO_3 production pathways. The gray shaded areas denote the possible ranges of $\delta^{15}N\text{-}\Delta^{17}O$ compositions of HNO_3 calculated using event-specific $\delta^{15}N\text{-}NO_x$ source signatures and a range of f_{NO2} and f_{O3} values (see Fig. 4 and text for more details). The dashed lines denote mixing among the three HNO_3 pathways and represent the border of the predicted $\delta^{15}N\text{-}\Delta^{17}O$ space.

$\delta^{18}O\text{-}NO_3^-$ values (Fig. 5). For example, on 9 July, $\delta^{18}O\text{-}NO_3^-$ values were lowest at the beginning of the event and increased sharply toward the end of the storm. In contrast, $\delta^{18}O\text{-}NO_3^-$ values were highest in the first samples collected on 26 September and decreased sharply at the end of that event (Fig. 5).

The temporal patterns in $\Delta^{17}O\text{-}NO_3^-$ were generally similar to those observed for $\delta^{18}O\text{-}NO_3^-$ (Fig. 5), where $\Delta^{17}O\text{-}NO_3^-$ values ranged from +11.2‰ to +30.6‰ across all events (Table 1) and were highly variable during individual storms. For example, $\Delta^{17}O\text{-}NO_3^-$ values on 9 July increased by 9‰ over a two-hour period, whereas during the 11 and 16 September events, $\Delta^{17}O\text{-}NO_3^-$ values decreased by approximately 9‰ over a two-hour period (Fig. 5).

The measured $\delta^{15}N\text{-}NO_3^-$ and $\Delta^{17}O\text{-}NO_3^-$ values for each storm were plotted within the $\delta^{15}N\text{-}\Delta^{17}O$ array parameterized using the predicted $\delta^{15}N\text{-}NO_x$ source signatures specific to each storm (Fig. 6). Within the $\delta^{15}N\text{-}\Delta^{17}O$ array, measured $\Delta^{17}O\text{-}NO_3^-$ values for all events generally coincided with the $\Delta^{17}O\text{-}NO_3^-$ range characteristic of the daytime $HNO_3(1)$ pathway with a f_{O3} value ranging approximately from 1 to 0.4 (Fig. 6). On 9 July, 26 September, 28 September, and 30 September, some of the measured $\delta^{15}N\text{-}NO_3^-$ values either plot within the range characteristic of the $HNO_3(1)$ pathway or represent a mixture of $HNO_3(1)$ and $HNO_3(3)$ pathways (Fig. 6). However, the measured $\delta^{15}N\text{-}NO_3^-$ values on 11 September and 16 September lie to the left (lower $\delta^{15}N$) of the $\delta^{15}N\text{-}\Delta^{17}O$ space that accounts for variability in both NO_x emission sources and chemistry effects (Fig. 6).

4. Discussion

The high degree of isotopic variability within individual storm events was surprising; to our knowledge, this is the first study to demonstrate such extreme variability in $\delta^{15}N$, $\delta^{18}O$, and $\Delta^{17}O$ over short time scales (Fig. 5). Moreover, the observed $\delta^{15}N\text{-}NO_3^-$ values were generally much lower than the predicted source $\delta^{15}N\text{-}NO_x$ based on the back-trajectory analysis (Fig. 6 and S2). Below we consider several factors related to isotopic fractionations during atmospheric NO_3^- formation as well as dynamic NO_x source effects that may have contributed to the highly variable and often low $\delta^{15}N$ values of precipitation NO_3^- we observed during storm events.

4.1. Isotopic fractionations during atmospheric NO_3^- formation

Isotopic fractionations during NO_x oxidation processes in the atmosphere may alter the $\delta^{15}N$ and $\delta^{18}O$ values of atmospheric NO_3^- from the original NO_x source isotopic signatures. Once NO is emitted and partially oxidized to NO_2 in the atmosphere, distribution of N isotopes between NO and NO_2 is controlled by an isotopic exchange equilibrium, which has recently been experimentally confirmed to have a large isotope effect ($\varepsilon_{eq(NO2/NO)}$ = 37‰ at 298 K) (Walters et al., 2016). As a result, when NO and NO_2 exist in comparable concentrations, ^{15}N is preferentially partitioned into NO_2 if N isotopic equilibrium is achieved, leading to higher $\delta^{15}N\text{-}NO_2$ relative to $\delta^{15}N\text{-}NO$ and $\delta^{15}N\text{-}NO_x$ (Freyer et al., 1993; Walters et al., 2016). Moreover, equilibrium N isotope exchange between NO_2, NO_3, and N_2O_5— the substrates for atmospheric HNO_3 production— was recently investigated using theoretical calculations by Walters and Michalski (2015). Based on these calculations, $\delta^{15}N\text{-}NO_3$ and $\delta^{15}N\text{-}N_2O_5$ are significantly lower (e.g., by 9‰ at 298 K) and higher (e.g., by 26‰ at 298 K), respectively, than $\delta^{15}N\text{-}NO_2$ if N isotopic equilibrium is achieved (Fig. 1). These calculated equilibrium isotope effects have been recently applied to correct the isotopic fractionations of NO_x during HNO_3 production for

source partitioning of particulate NO_3^- deposition using $\delta^{18}O\text{-}NO_3^-$ as an independent tracer of the HNO_3 production pathways (Chang et al., 2018; Zong et al., 2017).

In this study, the oxidation processes were constrained using the simultaneously measured $\Delta^{17}O$ of precipitation NO_3^-. As shown in Fig. 1, during atmospheric NO oxidation to NO_2, the $\Delta^{17}O$ value of NO_2 is determined by f_{O3} (Morin et al., 2011) and $\Delta^{17}O\text{-}O_3^*$, which has been experimentally quantified to range between 40‰ and 45‰ (Morin et al., 2011; Savarino et al., 2008; Vicars and Savarino, 2014). This $\Delta^{17}O\text{-}NO_2$ signal is further transferred to atmospheric NO_3^- along the three HNO_3 formation pathways that involve O_3 to different extents and thus have distinct $\Delta^{17}O$ transfer functions constrained by the oxygen mass balance (Fig. 1; Equations (7)–(9)). Therefore, $\Delta^{17}O\text{-}NO_3^-$ is a more robust tracer of the HNO_3 production pathways than $\delta^{18}O\text{-}NO_3^-$ because it is not altered by mass-dependent equilibrium and kinetic isotope effects during atmospheric reactions (Michalski et al., 2003). As shown in Fig. 6, although the measured $\Delta^{17}O\text{-}NO_3^-$ values within each precipitation event were temporally variable, the range of these values points to the daytime HNO_3(1) pathway (Reaction 4) as the dominant pathway for NO_x conversion to NO_3^-. This is consistent with previous $\Delta^{17}O\text{-}NO_3^-$-based deposition studies demonstrating that atmospheric NO_3^- is mainly formed through the HNO_3(1) pathway during summer in temperate areas (Alexander et al., 2009; Michalski et al., 2003).

However, while the observed $\Delta^{17}O\text{-}NO_3^-$ values point to the HNO_3(1) pathway as the dominant source of precipitation NO_3^-, most of the measured $\delta^{15}N$ values shown in Fig. 6 fall outside the space bounded by the three HNO_3 formation pathways, suggesting that the high degree of variability in observed $\delta^{15}N\text{-}NO_3^-$ values cannot be fully explained by the back trajectory $\delta^{15}N\text{-}NO_x$ source signatures and/or equilibrium isotope effects associated with HNO_3 production. Importantly, kinetic isotope effects associated with NO_x oxidation and HNO_3 formation pathways are not included in the proposed $\delta^{15}N\text{-}\Delta^{17}O$ array because the magnitudes of these isotope effects remain poorly constrained. Using *ab initio* calculations, Walters and Michalski (2016) reported that the oxidation of NO to NO_2 via O_3 is associated with a kinetic N isotope effect ($\varepsilon_{k(NO2/NO)}$) of −7‰ (at 298 K), indicating that the produced NO_2 from Reaction 1 and, subsequently, NO_3^- produced from the HNO_3(1) pathway may have a $\delta^{15}N$ value lower than NO and total NO_x. Thus, to some extent the $\delta^{15}N$ of NO_3^- produced from the HNO_3(1) pathway likely depends on atmospheric conditions (e.g., temperature, radiation, and oxidant availability) that determine the limiting step during photochemical NO_x oxidation (Freyer et al., 1993; Walters et al., 2016) and may be lower than the predicted $\delta^{15}N\text{-}HNO_3$ value based on the equilibrium isotope effects alone. Moreover, the final step in NO_3^- formation in the HNO_3(1) pathways (Reaction 4; i.e., NO_2 + OH) may also be associated with potentially numerous kinetic isotope effects, depending on whether the HNO_3 product behaves as a permanent sink for NO_2 (e.g., via infiltration of wet-deposited HNO_3 into the soil) or, alternatively, undergoes post-depositional photochemically-mediated "renoxification" (Ndour et al., 2009; Reed et al., 2017; Zhou et al., 2003). Freyer (1991) suggested the conversion of NO_2 to HNO_3 would have a kinetic isotope effect of approximately −3‰ based on diffusion rates of $^{15}NO_2$ relative to $^{14}NO_2$. While further theoretical and experimental constraints are needed to confirm this assumed kinetic isotope effect and also to quantify the potential influence of renoxification processes on the overall kinetic isotope effects associated with this reaction, this early work emphasizes the potentially important role of Reaction 4 in controlling $\delta^{15}N$ of NO_3^- produced from the HNO_3(1) pathway, beyond the N isotopic partitioning between NO and NO_2.

Nevertheless, although kinetic isotope effects may systematically shift the $\delta^{15}N\text{-}NO_3^-$ values from $\delta^{15}N\text{-}NO_x$ source signatures, it is unlikely that these would result in the high degree of variability we observed in $\delta^{15}N\text{-}NO_3^-$ values within individual precipitation events. For example, on 9 July, $\delta^{15}N\text{-}NO_3^-$ values varied up to 16‰ over 2 h (Fig. 5; Fig. S2). Such large short-term variation in $\delta^{15}N\text{-}NO_3^-$ cannot be explained by the anticipated kinetic isotope effects (i.e., 3–7‰), even assuming that these kinetic isotope effects were fully expressed during the NO_x-to-HNO_3 conversion. Furthermore, except for the 28 September event, when $\delta^{15}N$ values decreased significantly with increasing precipitation intensity ($R^2 = 0.82$; $p = 0.0049$), precipitation intensity at Fernow was not significantly correlated with NO_3^- concentration, $\delta^{15}N$, $\delta^{18}O$, or $\Delta^{17}O$ during any storm. This absence of significant correlation suggests that kinetic fractionation effects resulting from physical processes during storms (e.g., rainout and washout) might have only a minor impact on the measured $\delta^{15}N\text{-}NO_3^-$ values. Therefore, we conclude that although interpreting precipitation NO_3^- using the proposed $\delta^{15}N\text{-}\Delta^{17}O$ provides unique insights into the atmospheric NO_3^- formation pathways, considering only the chemically- and physically-driven N isotopic fractionations is insufficient to fully resolve the low values and extreme variability of $\delta^{15}N\text{-}NO_3^-$ measured during individual storm events.

4.2. Dynamic source effects on triple isotopes of precipitation NO_3^-

Previous studies of $\delta^{15}N$ measured in atmospheric NO_3^- have assumed that the N isotopic compositions of NO_x sources are retained during oxidation to NO_3^- or, alternatively, that equilibrium and kinetic isotope effects that might alter $\delta^{15}N\text{-}NO_x$ values during oxidation reactions are smaller than the differences in $\delta^{15}N$ values among NO_x sources (Elliott et al., 2009, 2007; Felix et al., 2015; Freyer, 1991; Hastings et al., 2003; Walters et al., 2018). Thus, $\delta^{15}N$ has been considered a viable tracer of NO_x source contributions to atmospheric NO_3^-; the positive linear relationships between total EGU NO_x emissions and $\delta^{15}N\text{-}NO_3^-$ values in precipitation measured during some storms support this idea. However, the $\delta^{15}N\text{-}NO_3^-$ values we measured in precipitation are generally lower than the predicted $\delta^{15}N\text{-}NO_x$ values based on back trajectory source contributions by up to 22‰ (Fig. 6 and S2). Given that these lower $\delta^{15}N\text{-}NO_3^-$ values cannot be fully explained by the equilibrium and kinetic isotope effects associated with the NO_x-to-HNO_3 conversion (see above), they may suggest a missing source contribution during the back trajectory analysis.

The low $\delta^{15}N\text{-}NO_3^-$ values measured during precipitation events may be attributable to the spatio-temporal scale of the NEI emissions data for vehicle and biogenic sources used in this study. Estimates of total hourly NO_x from these sources were calculated from modeled monthly values aggregated to the county-level; these estimates may be too spatially coarse and temporally smoothed to provide adequate estimates of NO_x emissions from these sources on time scales as short as individual storms. In contrast, back trajectory EGU emissions data were based on hourly, unit level NO_x emission measurements taken from individual EGUs, and emissions were temporally and spatially linked such that only those NO_x emissions occurring at the time the projected air mass was passing over a particular EGU were included in the calculation of total EGU NO_x emissions. This discrepancy in the scale of detailed measurements available for NO_x sources may have contributed to the stronger relationships between $\delta^{15}N\text{-}NO_3^-$ and NO_x emissions observed for EGUs. Improved constraints on the spatio-temporal emission and deposition dynamics of all NO_x sources considered in this study would facilitate a better understanding of the influence these factors exert on the isotopic composition of atmospheric NO_3^-, particularly on short time scales. However, prior work on near road deposition and regional isoscapes has suggested significant N deposition in near-road environments (Ammann et al., 1999; Cape et al., 2004; Redling et al., 2013). NO_x emitted from vehicle exhaust and biogenic sources may therefore exhibit different transport and deposition dynamics than NO_x emitted higher in the boundary layer (e.g., from EGU stacks), resulting in relatively small contributions of these near-surface sources to NO_3^- deposition in down-wind areas.

Based on these considerations, we therefore suggest that biogenic NO_x pulses from soils and their interaction with the forest canopy may affect the isotopic composition and temporal variability of precipitation

$\delta^{15}N\text{-}NO_3^-$ more strongly than previously recognized. Indeed, substantial plumes of microbial NO_x have been observed across a wide variety of land use types, particularly following soil wetting (Davidson et al., 2000; Davidson and Kingerlee, 1997; Ghude et al., 2010; Hudman et al., 2012; Jaeglé et al., 2004; Stark et al., 2002; Zhang et al., 2011). Due to the low $\delta^{15}N$ values of biogenic NO_x (−59.8‰ to −19.9‰ (Felix and Elliott, 2013; Li and Wang, 2008; Yu and Elliott, 2017)), even small contributions from this source could cause large shifts in $\delta^{15}N\text{-}NO_3^-$ on short time scales. Using a dynamic soil chamber system (Yu and Elliott, 2017), recently measured the rate and $\delta^{15}N$ of soil NO emissions in an urban soil plot subjected to a 2-week drying period. Upon re-wetting of the soil with deionized water, pulsed emission of $\delta^{15}N$-depleted NO (−42‰) was triggered and sustained at about 0.1 mg $m^{-2}{\cdot}h^{-1}$ over the following 7 h (Yu and Elliott, 2017). Upscaling this pulsed NO emission to the 100 km buffer area used in our study results in a total NO_x emission of about 190 tons$\cdot d^{-1}$. This estimated NO emission is comparable to the total NO_x emissions from EGUs, vehicles, and biogenic sources along 24-h air mass back trajectories for the six storm events (i.e., 18–261 tons$\cdot d^{-1}$, Table S2). Although *in situ* measurements would be required to constrain the specific soil NO emission rates at Fernow, the recent experimental evidence of (Yu and Elliott, 2017) suggests that soil NO pulses could be large enough in some cases to substantially contribute to the variability in $\delta^{15}N$ values of precipitation NO_3^-. Other isotope-based studies have suggested that biogenic NO_x may account for as much as 15% of ambient NO_2 measured during the summertime in the midwestern U.S. (Walters et al., 2018); in contrast, model estimated biogenic NO_x emissions along back trajectories in our study represented only 0.4% of total NO_x emissions across all storms. The coarse scale of NEI-based biogenic NO_x emission estimates used in this study, along with the potential effects of interactions between soil NO_x emissions and the forest canopy (discussed below), may have led to an underestimation of biogenic source contributions to total NO_x along back trajectories.

The idea of soil NO_x emissions as a localized contributor to precipitation NO_3^- at Fernow is also consistent with the range of $\Delta^{17}O\text{-}NO_3^-$ values we observed. To our knowledge, this study is the first to report $\Delta^{17}O\text{-}NO_3^-$ values as low as +11.2‰ in precipitation. While such low $\Delta^{17}O$ values have not been widely reported for precipitation NO_3^-, the convergence of several environmental conditions likely present at our study site may have resulted in the low $\Delta^{17}O$ and $\delta^{15}N$ values we observed. First, suppressed O_3 production under cloudy conditions during storms may have reduced NO_x oxidation via O_3. More importantly, previous work in forested systems has suggested that complex interactions among soil NO emissions, forest canopy surfaces, and VOCs emitted from vegetation can lead to the accumulation of NO_2, OH, gaseous HNO_3, and particulate NO_3^- within and below the forest canopy (Farmer and Cohen, 2008; Ganzeveld et al., 2002; Gao et al., 1993; Geddes and Murphy, 2014; Makar et al., 2017). The densely-forested surroundings near our sampling location, combined with the full canopy leaf-out conditions at the site during the growing season period, may have facilitated interactions between biogenic NO and hydroxyl and organo-peroxy radicals, resulting in an accumulation of gaseous HNO_3 and particulate NO_3^- with low $\Delta^{17}O$ and $\delta^{15}N$ values within and below the forest canopy between rainfall events. This biogenically-sourced atmospheric NO_3^- could have undergone rapid removal from the atmosphere and from leaf surfaces through below cloud scavenging processes (i.e., washout) during subsequent rainfall events, contributing to the low and extremely variable $\delta^{15}N$ and $\Delta^{17}O$ values we observed in precipitation NO_3^-. This conclusion is consistent with a previous study adopting a similar high-frequency measurement technique (Felix et al., 2015). In sequential rainfall samples collected during Hurricane Irene, Felix et al. (2015) observed the lowest $\delta^{15}N\text{-}NO_3^-$ values (−5.5‰ and −5.7‰) in samples with a significant terrestrial back trajectory component; the authors suggested that biogenic NO_x emissions may have influenced the isotopic composition of these samples, as $\delta^{15}N\text{-}NO_3^-$ values were also correlated with high concentrations of the biogenic compounds acetaldehyde and ethanol in precipitation. It is also possible that some portion of the HNO_3 deposited on leaf surfaces was photochemically converted to HONO and NO_2 via renoxification during sunlit periods between storm events (Ndour et al., 2009; Reed et al., 2017; Zhou et al., 2003). The relative importance of such processes during rainfall events has not been investigated and their isotopic effects are also currently unknown; additional work in these areas would provide critical insight into the interpretation of nitrate isotopic variability on short time scales.

5. Conclusions and implications

The wide range of $\Delta^{17}O\text{-}NO_3^-$ values encompassed by the precipitation NO_3^- measured during these growing season storms and the variability in $\delta^{15}N$ and $\delta^{18}O$ of NO_3^- over short time periods demonstrate the complex nature of atmospheric NO_3^- formation and deposition processes during storm events, and the utility of triple NO_3^- isotopes for understanding these processes. The findings of this study suggest that while regional EGU NO_x emissions are an important source of atmospheric NO_3^- at Fernow, local biogenic NO_x emissions as well as oxidation processes and kinetic and equilibrium fractionation effects may also play an important— albeit poorly constrained— role in the isotopic variability of atmospheric NO_3^- on short time scales. Given the extreme isotopic variability observed on hourly time scales in this study, precipitation sampling conducted over longer time scales (i.e., bulk sampling of an entire event or integrated weekly sampling) may be inadequate to fully characterize the dynamic nature of NO_x source contributions and oxidation processes during atmospheric NO_3^- formation. The results of our field-based study are in agreement with previous field-based studies that have characterized the $\delta^{15}N$ and $\delta^{18}O$ isotopic composition of precipitation NO_3^- (Buda and DeWalle, 2009; Felix et al., 2015; Liu et al., 2017) and suggest that our current understanding of isotopic fractionations during the atmospheric NO_x-to-HNO_3 conversion is still incomplete. Future efforts should be dedicated to constraining kinetic isotope effects associated with various steps of atmospheric NO_3^- formation to better understand how $\delta^{15}N\text{-}NO_x$ source signatures are altered by atmospheric processes under varying conditions. Furthermore, our data suggest that biogenic NO_x emissions may play a more important role in determining the N and O isotopic composition of precipitation NO_3^- than previously thought. It is therefore critical that future work focus on improving the constraints on biogenic NO_x emission and forest canopy effects on NO_3^- stable isotopes in order to better clarify their roles in atmospheric NO_3^- formation and deposition processes.

Declarations of interest

None.

Acknowledgements

This work was supported by NSF grant #0910521 to EME and Agriculture and Food Research Initiative grant #2012-67011-19663 from the USDA National Institute of Food and Agriculture to LAR. We thank Stephen Rose for assistance with sample collection, Mary Beth Adams and Chris Cassidy for assistance with site access at Fernow, and Katherine Redling for assistance with isotopic analysis.

Appendix A. Supplementary data

Supplementary data to this article can be found online at https://doi.org/10.1016/j.atmosenv.2019.03.012.

References

Alexander, B., Hastings, M.G., Allman, D.J., Dachs, J., Thornton, J.A., Kunasek, S.A., 2009. Quantifying atmospheric nitrate formation pathways based on a global model of the oxygen isotopic composition (^{17}O) of atmospheric nitrate. Atmos. Chem. Phys. 9, 5043–5056. https://doi.org/10.5194/acp-9-5043-2009.

AMEC Environment & Infrastructure, Inc (AMEC), 2012. Clean Air Status and Trends Network (CASTNET) 2010 Annual Report. Prepared for U.S. Environmental Protection Agency (EPA), Office of Air and Radiation, Clean Air Markets Division, Washington, DC (Contract No. EP-W-09-028. Gainesville, FL.

Ammann, M., Siegwolf, R., Pichlmayer, F., Suter, M., Saurer, M., Brunold, C., 1999. Estimating the uptake of traffic-derived NO_2 from ^{15}N abundance in Norway spruce needles. Oecologia 118, 124–131. https://doi.org/10.1007/s004420050710.

Baek, B.H., Aneja, V.P., Tong, Q., 2004. Chemical coupling between ammonia, acid gases, and fine particles. Environ. Pollut. 129, 89–98. https://doi.org/10.1016/j.envpol.2003.09.022.

Behera, S.N., Sharma, M., 2010. Investigating the potential role of ammonia in ion chemistry of fine particulate matter formation for an urban environment. Sci. Total Environ. 408, 3569–3575. https://doi.org/10.1016/j.scitotenv.2010.04.017Cape.

Buda, A.R., DeWalle, D.R., 2009. Using atmospheric chemistry and storm track information to explain the variation of nitrate stable isotopes in precipitation at a site in central Pennsylvania, USA. Atmos. Environ. 43, 4453–4464. https://doi.org/10.1016/j.atmosenv.2009.06.027.

Cape, J.N., Tang, Y.S., Van Dijk, N., Love, L., Sutton, M.A., Palmer, S.C.F., 2004. Concentrations of ammonia and nitrogen dioxide at roadside verges, and their contribution to nitrogen deposition. Environ. Pollut. 132, 469–478. https://doi.org/10.1016/j.envpol.2004.05.009.

Carter, J.F., Fry, B., 2013. Ensuring the reliability of stable isotope ratio data- beyond the principle of identical treatment. Anal. Bioanal. Chem. 405, 2799–2814. https://doi.org/10.1007/s00216-012-6551-0.

Casciotti, K.L., Sigman, D.M., Hastings, M.G., Böhlke, J.K., Hilkert, A., 2002. Measurement of the oxygen isotopic composition of nitrate in seawater and freshwater using the denitrifier method. Anal. Chem. 74, 4905–4912. https://doi.org/10.1021/ac020113w.

Chang, Y., Zhang, Y., Tian, C., Zhang, S., Ma, X., Cao, F., Liu, X., Zhang, W., Kuhn, T., Lehmann, M.F., 2018. Nitrogen isotope fractionation during gas-to-particle conversion of NO_x to NO_3^- in the atmosphere–implications for isotope-based NO_x source apportionment. Atmos. Chem. Phys. 18, 11647–11661. https://doi.org/10.5194/acp-18-11647-2018.

Coplen, T.B., Böhlke, J.K., Casciotti, K.L., 2004. Using dual-bacterial denitrification to improve $\delta^{15}N$ determinations of nitrates containing mass-independent ^{17}O. Rapid Commun. Mass Spectrom. 18, 245–250. https://doi.org/10.1002/rcm.1318.

Davidson, E.A., Kingerlee, W., 1997. A global inventory of nitric oxide emissions from soils. Nutrient Cycl. Agroecosyst. 48, 37–50. https://doi.org/10.1023/A:1009738715891.

Davidson, E.A., Keller, M., Erickson, H.E., Verchot, L.V., Veldkamp, E., 2000. Testing a conceptual model of soil emissions of nitrous and nitric oxides. BioScience 50, 667–680. https://doi.org/10.1641/0006-3568(2000)050[0667:TACMOS]2.0.CO;2.

De Gouw, J.A., Parrish, D.D., Frost, G.J., Trainer, M., 2014. Reduced emissions of CO_2, NO_x, and SO_2 from US power plants owing to switch from coal to natural gas with combined cycle technology. Earths Future 2, 75–82. https://doi.org/10.1002/2013EF000196.

Driscoll, C.T., Lawrence, G.B., Bulger, A.J., Butler, T.J., Cronan, C.S., Eagar, C., Lambert, K.F., Likens, G.E., Stoddard, J.L., Weathers, K.C., 2001. Acidic deposition in the northeastern United States: sources and inputs, ecosystem effects, and management strategies. BioScience 51, 180–198. [0180:ADITNU]2.0.CO;2. https://doi.org/10.1641/0006-3568(2001)051.

Elliott, E.M., Kendall, C., Wankel, S.D., Burns, D.A., Boyer, E.W., Harlin, K., Bain, D.J., Butler, T.J., 2007. Nitrogen isotopes as indicators of NO_x source contributions to atmospheric nitrate deposition across the midwestern and northeastern United States. Environ. Sci. Technol. 41, 7661–7667. https://doi.org/10.1021/es070898t.

Elliott, E.M., Kendall, C., Boyer, E.W., Burns, D.A., Lear, G.G., Golden, H.E., Harlin, K., Bytnerowicz, A., Butler, T.J., Glatz, R., 2009. Dual nitrate isotopes in dry deposition: utility for partitioning NO_x source contributions to landscape nitrogen deposition. J. Geophys. Res. 114, G04020. https://doi.org/10.1029/2008JG000889.

Elliott, E.M., Yu, Z., Cole, A.S., Coughlin, J.G., 2019. Isotopic advances in understanding reactive nitrogen deposition and atmospheric processing. Sci. Total Environ. 662, 393–403. https://doi.org/10.1016/j.scitotenv.2018.12.177.

Farmer, D.K., Cohen, R.C., 2008. Observations of HNO_3, ΣAN, ΣPN and NO_2 fluxes: evidence for rapid HO_x chemistry within a pine forest canopy. Atmos. Chem. Phys. 8, 3899–3917. https://doi.org/10.5194/acp-8-3899-2008.

Felix, J.D., Elliott, E.M., 2013. The agricultural history of human-nitrogen interactions as recorded in ice core $\delta^{15}N$-NO_3^-. Geophys. Res. Lett. 40, 1642–1646. https://doi.org/10.1002/grl.50209.

Felix, J.D., Elliott, E.M., 2014. Isotopic composition of passively collected nitrogen dioxide emissions: vehicle, soil and livestock source signatures. Atmos. Environ. 359–366. https://doi.org/10.1016/j.atmosenv.2014.04.005.

Felix, J.D., Elliott, E.M., Shaw, S.L., 2012. Nitrogen isotopic composition of coal-fired power plant NO_x: influence of emission controls and implications for global emission inventories. Environ. Sci. Technol. 46, 3528–3535. https://doi.org/10.1021/es203355v.

Felix, J.D., Elliott, E.M., Avery, G.B., Kieber, R.J., Mead, R.N., Willey, J.D., Mullaugh, K.M., 2015. Isotopic composition of nitrate in sequential Hurricane Irene precipitation samples: implications for changing NO_x sources. Atmos. Environ. 106, 191–195. https://doi.org/10.1016/j.atmosenv.2015.01.075.

Finlayson-Pitts, B.J., Pitts Jr., J.N., 1999. Chemistry of the Upper and Lower Atmosphere: Theory, Experiments, and Applications. Elsevier, San Diego.

Freyer, H.D., 1991. Seasonal variation of $^{15}N/^{14}N$ ratios in atmospheric nitrate species. Tellus B 43, 30–44. https://doi.org/10.1034/j.1600-0889.1991.00003.x.

Freyer, H.D., Kley, D., Volz-Thomas, A., Kobel, K., 1993. On the interaction of isotopic exchange processes with photochemical reactions in atmospheric oxides of nitrogen. J. Geophys. Res. Atmospheres 98, 14791–14796. https://doi.org/10.1029/93JD00874.

Ganzeveld, L.N., Lelieveld, J., Dentener, F.J., Krol, M.C., Bouwman, A.J., Roelofs, G.J., 2002. Global soil-biogenic NO_x emissions and the role of canopy processes. J. Geophys. Res. 107, 4298. https://doi.org/10.1029/2001JD001289.

Gao, W., Wesely, M.L., Doskey, P.V., 1993. Numerical modeling of the turbulent diffusion and chemistry of NO_x, O_3, isoprene, and other reactive trace gases in and above a forest canopy. J. Geophys. Res. Atmospheres 98, 18339–18353. https://doi.org/10.1029/93JD01862.

Geddes, J.A., Murphy, J.G., 2014. Observations of reactive nitrogen oxide fluxes by eddy covariance above two midlatitude North American mixed hardwood forests. Atmos. Chem. Phys. 14, 2939–2957. https://doi.org/10.5194/acp-14-2939-2014.

Ghude, S.D., Lal, D.M., Beig, G., 2010. Rain-induced soil NO_x emission from India during the onset of the summer monsoon: a satellite perspective. J. Geophys. Res. 115, D16304. https://doi.org/10.1029/2009JD013367.

Grennfelt, P., Hultberg, H., 1986. Effects of nitrogen deposition on the acidification of terrestrial and aquatic ecosystems. Water Air Soil Pollut. 30, 945–963. https://doi.org/10.1007/978-94-009-3385-9_96.

Hastings, M.G., Sigman, D.M., Lipschultz, F., 2003. Isotopic evidence for source changes of nitrate in rain at Bermuda. J. Geophys. Res. 108, 4790. https://doi.org/10.1029/2003JD003789.

Heaton, T.H.E., 1990. $^{15}N/^{14}N$ ratios of NO_x from vehicle engines and coal-fired power stations. Tellus B 42, 304–307. https://doi.org/10.1034/j.1600-0889.1990.00007.x-i1.

Hudman, R.C., Moore, N.E., Mebust, A.K., Martin, R.V., Russell, A.R., Valin, L.C., Cohen, R.C., 2012. Steps towards a mechanistic model of global soil nitric oxide emissions: implementation and space based-constraints. Atmos. Chem. Phys. Discuss. 12, 3555–3594. https://doi.org/10.5194/acp-12-7779-2012.

Jaeglé, L., Martin, R.V., Chance, K., Steinberger, L., Kurosu, T.P., Jacob, D.J., Modi, A.I., Yoboué, V., Sigha-Nkamdjou, L., Galy-Lacaux, C., 2004. Satellite mapping of rain-induced nitric oxide emissions from soils. J. Geophys. Res. 109, D21310. https://doi.org/10.1029/2004JD004787.

Kaiser, J., Hastings, M.G., Houlton, B.Z., Röckmann, T., Sigman, D.M., 2007. Triple oxygen isotope analysis of nitrate using the denitrifier method and thermal decomposition of N_2O. Anal. Chem. 79, 599–607. https://doi.org/10.1021/ac061022s.

Kendall, C., Elliott, E.M., Wankel, S.D., 2007. Tracing anthropogenic inputs of nitrogen to ecosystems. In: Michener, R., Lajtha, K. (Eds.), Stable Isotopes in Ecology and Environmental Science. Blackwell Publishing, Oxford, pp. 375–449.

Kim, S.-W., Heckel, A., McKeen, S.A., Frost, G.J., Hsie, E.-Y., Trainer, M.K., Richter, A., Burrows, J.P., Peckham, S.E., Grell, G.A., 2006. Satellite-observed US power plant NO_x emission reductions and their impact on air quality. Geophys. Res. Lett. 33, L22812. https://doi.org/10.1029/2006GL027749.

Kochenderfer, J.N., 2007. Fernow and the Appalachian hardwood region. In: Adams, M.B., DeWalle, D.R., Hom, J.R. (Eds.), The Fernow Watershed Acidification Study. Springer, Dordrecht, The Netherlands, pp. 17–39.

Lamsal, L.N., Martin, R.V., Van Donkelaar, A., Celarier, E.A., Bucsela, E.J., Boersma, K.F., Dirksen, R., Luo, C., Wang, Y., 2010. Indirect validation of tropospheric nitrogen dioxide retrieved from the OMI satellite instrument: insight into the seasonal variation of nitrogen oxides at northern midlatitudes. J. Geophys. Res. Atmospheres 115 1984–2012. https://doi.org/10.1029/2009JD013351.

Levy, H., Moxim, W.J., Klonecki, A.A., Kasibhatla, P.S., 1999. Simulated tropospheric NO_x: its evaluation, global distribution and individual source contributions. J. Geophys. Res. Atmospheres 104, 26279–26306. https://doi.org/10.1029/1999JD900442.

Li, D., Wang, X., 2008. Nitrogen isotopic signature of soil-released nitric oxide (NO) after fertilizer application. Atmos. Environ. 42, 4747–4754. https://doi.org/10.1016/j.atmosenv.2008.01.042.

Liu, X.-Y., Xiao, H.-W., Xiao, H.-Y., Song, W., Sun, X.-C., Zheng, X.-D., Liu, C.-Q., Koba, K., 2017. Stable isotope analyses of precipitation nitrogen sources in Guiyang, southwestern China. Environ. Pollut. 230, 486–494. https://doi.org/10.1016/j.envpol.2017.06.010.

Makar, P.A., Staebler, R.M., Akingunola, A., Zhang, J., McLinden, C., Kharol, S.K., Pabla, B., Cheung, P., Zheng, Q., 2017. The effects of forest canopy shading and turbulence on boundary layer ozone. Nat. Commun. 8, 15243. https://doi.org/10.1038/ncomms15243.

Michalski, G., Bhattacharya, S.K., 2009. The role of symmetry in the mass independent isotope effect in ozone. Proc. Natl. Acad. Sci. Unit. States Am. 106, 5493–5496. https://doi.org/10.1073/pnas.0812755106.

Michalski, G., Scott, Z., Kabiling, M., Thiemens, M.H., 2003. First measurements and modeling of $\Delta^{17}O$ in atmospheric nitrate. Geophys. Res. Lett. 30, 1870. https://doi.org/10.1029/2003GL017015.

Michalski, G., Bhattacharya, S.K., Girsch, G., 2014. NO_x cycle and the tropospheric ozone isotope anomaly: an experimental investigation. Atmos. Chem. Phys. 14, 4935–4953. https://doi.org/10.5194/acp-14-4935-2014.

Miller, D.J., Wojtal, P.K., Clark, S.C., Hastings, M.G., 2017. Vehicle NO_x emission plume

isotopic signatures: spatial variability across the eastern United States. J. Geophys. Res. Atmospheres 122, 4698–4717. https://doi.org/10.1002/2016JD025877.
Morin, S., Savarino, J., Frey, M.M., Domine, F., Jacobi, H.-W., Kaleschke, L., Martins, J.M., 2009. Comprehensive isotopic composition of atmospheric nitrate in the Atlantic Ocean boundary layer from 65 S to 79 N. J. Geophys. Res. Atmospheres 114, D05303.
Morin, S., Sander, R., Savarino, J., 2011. Simulation of the diurnal variations of the oxygen isotope anomaly ($\Delta^{17}O$) of reactive atmospheric species. Atmos. Chem. Phys. 11, 3653–3671. https://doi.org/10.5194/acp-11-3653-2011.
Munger, J.W., Fan, S.-M., Bakwin, P.S., Goulden, M.L., Goldstein, A., Colman, A.S., Wofsy, S.C., 1998. Regional budgets for nitrogen oxides from continental sources: variations of rates for oxidation and deposition with season and distance from source regions. J. Geophys. Res. Atmospheres 103, 8355–8368. https://doi.org/10.1029/98JD00168.
National Atmospheric Deposition Program, 2011. National Atmospheric Deposition Program 2010 Annual Summary (No. NADP Data Report 2011-01). Illinois State Water Survey, Urbana IL.
Ndour, M., Conchon, P., D'Anna, B., Ka, O., George, C., 2009. Photochemistry of mineral dust surface as a potential atmospheric renoxification process. Geophys. Res. Lett. 36, L05816. https://doi.org/10.1029/2008GL036662.
Proemse, B.C., Mayer, B., Chow, J.C., Watson, J.G., 2012. Isotopic characterization of nitrate, ammonium and sulfate in stack PM2.5 emissions in the Athabasca Oil Sands Region, Alberta, Canada. Atmos. Environ. 60, 555–563. https://doi.org/10.1016/j.atmosenv.2012.06.046.
Redling, K., Elliott, E., Bain, D., Sherwell, J., 2013. Highway contributions to reactive nitrogen deposition: tracing the fate of vehicular NO_x using stable isotopes and plant biomonitors. Biogeochemistry 116, 261–274. https://doi.org/10.1007/s10533-013-9857-x.
Reed, C., Evans, M.J., Crilley, L.R., Bloss, W.J., Sherwen, T., Read, K.A., Lee, J.D., Carpenter, L.J., 2017. Evidence for renoxification in the tropical marine boundary layer. Atmos. Chem. Phys. 17, 4081–4092. https://doi.org/10.5194/acp-17-4081-2017.
Revesz, K., Böhlke, J.-K., 2002. Comparison of $\delta^{18}O$ measurements in nitrate by different combustion techniques. Anal. Chem. 74, 5410–5413. https://doi.org/10.1021/ac025854b.
Savarino, J., Kaiser, J., Morin, S., Sigman, D.M., Thiemens, M.H., 2007. Nitrogen and oxygen isotopic constraints on the origin of atmospheric nitrate in coastal Antarctica. Atmos. Chem. Phys. 7, 1925–1945. https://doi.org/10.5194/acp-7-1925-2007.
Savarino, J., Bhattacharya, S.K., Morin, S., Baroni, M., Doussin, J.-F., 2008. The $NO + O_3$ reaction: a triple oxygen isotope perspective on the reaction dynamics and atmospheric implications for the transfer of the ozone isotope anomaly. J. Chem. Phys. 128, 194303. https://doi.org/10.1063/1.2917581.
Savarino, J., Morin, S., Erbland, J., Grannec, F., Patey, M.D., Vicars, W., Alexander, B., Achterberg, E.P., 2013. Isotopic composition of atmospheric nitrate in a tropical marine boundary layer. Proc. Natl. Acad. Sci. Unit. States Am. 110, 17668–17673. https://doi.org/10.1073/pnas.1216639110.
Schwede, D.B., Simpson, D., Tan, J., Fu, J.S., Dentener, F., Du, E., 2018. Spatial variation of modelled total, dry and wet nitrogen deposition to forests at global scale. Environ. Pollut. 243, 1287–1301. https://doi.org/10.1016/j.envpol.2018.09.084.
Seinfeld, J.H., Pandis, S.N., 2006. Atmospheric Chemistry and Physics. John Wiley & Sons, Hoboken, NJ.
Sigman, D.M., Casciotti, K.L., Andreani, M., Barford, C., Galanter, M., Böhlke, J.K., 2001. A bacterial method for the nitrogen isotopic analysis of nitrate in seawater and freshwater. Anal. Chem. 73, 4145–4153. https://doi.org/10.1021/ac010088e.
Stark, J.M., Smart, D.R., Hart, S.C., Haubensak, K.A., 2002. Regulation of nitric oxide emissions from forest and rangeland soils of western North America. Ecology 83, 2278–2292. [2278:RONOEF]2.0.CO;2. https://doi.org/10.1890/0012-9658(2002)083.
Sun, J., Fu, J.S., Huang, K., 2016. Organic nitrates and other oxidized nitrogen compounds contribute significantly to the total nitrogen depositions in the United States. Proc. Natl. Acad. Sci. Unit. States Am. 113, E4433–E4434. https://doi.org/10.1073/pnas.1608717113.
Thiemens, M.H., 2006. History and applications of mass-independent isotope effects. Annu. Rev. Earth Planet Sci. 34, 217–262. https://doi.org/10.1146/annurev.earth.34.031405.125026.
U.S. Environmental Protection Agency, 2008. 2008 National Emissions Inventory. [WWW Document]. 2008 Natl. Emiss. Inventory. http://www3.epa.gov/ttnchie1/net/2008inventory.html accessed 2.2.12.
U.S. Environmental Protection Agency, 2011. 2011 National emissions inventory data. [WWW Document]. https://www.epa.gov/air-emissions-inventories/2011-national-emissions-inventory-nei-data accessed 6.27.18.
U.S. Environmental Protection Agency, 2015. Air Markets Program database. [WWW Document]. Air Mark. Program. http://ampd.epa.gov/ampd accessed 2.2.12.
Vicars, W.C., Savarino, J., 2014. Quantitative constraints on the ^{17}O-excess ($\Delta^{17}O$) signature of surface ozone: ambient measurements from 50° N to 50° S using the nitrite-coated filter technique. Geochem. Cosmochim. Acta 135, 270–287. https://doi.org/10.1016/j.gca.2014.03.023.
Vicars, W.C., Morin, S., Savarino, J., Wagner, N.L., Erbland, J., Vince, E., Martins, J.M.F., Lerner, B.M., Quinn, P.K., Coffman, D.J., Williams, E.J., Brown, S.S., 2013. Spatial and diurnal variability in reactive nitrogen oxide chemistry as reflected in the isotopic composition of atmospheric nitrate: results from the CalNex 2010 field study. J. Geophys. Res. Atmospheres 118, 10567–10588. https://doi.org/10.1002/jgrd.50680.
Vitousek, P.M., Aber, J.D., Howarth, R.W., Likens, G.E., Matson, P.A., Schindler, D.W., Schlesinger, W.H., Tilman, D.G., 1997. Human alteration of the global nitrogen cycle: sources and consequences. Ecol. Appl. 7, 737–750 https://doi.org/10.1890/1051-0761(1997)007[0737:HAOTGN]2.0.CO;2.
Walters, W.W., Michalski, G., 2015. Theoretical calculation of nitrogen equilibrium isotope exchange fractionation factors for various NO_y molecules. Geochem. Cosmochim. Acta 164, 284–297. https://doi.org/10.1016/j.gca.2015.05.029.
Walters, W.W., Michalski, G., 2016. Theoretical calculation of oxygen equilibrium isotope fractionation factors involving various NO_y molecules, OH, and H_2O and its implications for isotope variations in atmospheric nitrate. Geochem. Cosmochim. Acta 191, 89–101. https://doi.org/10.1016/j.gca.2016.06.039.
Walters, W.W., Goodwin, S.R., Michalski, G., 2015. Nitrogen stable isotope composition ($\delta^{15}N$) of vehicle-emitted NO_x. Environ. Sci. Technol. 49, 2278–2285. https://doi.org/10.1021/es505580v.
Walters, W.W., Simonini, D.S., Michalski, G., 2016. Nitrogen isotope exchange between NO and NO_2 and its implications for $\delta^{15}N$ variations in tropospheric NO_x and atmospheric nitrate. Geophys. Res. Lett. 43, 440–448. https://doi.org/10.1002/2015GL066438.
Walters, W.W., Fang, H., Michalski, G., 2018. Summertime diurnal variations in the isotopic composition of atmospheric nitrogen dioxide at a small midwestern United States city. Atmos. Environ. 179, 1–11. https://doi.org/10.1016/j.atmosenv.2018.01.047.
Warby, R.A., Johnson, C.E., Driscoll, C.T., 2009. Continuing acidification of organic soils across the northeastern USA: 1984–2001. Soil Sci. Soc. Am. J. 73, 274–284. https://doi.org/10.2136/sssaj2007.0016.
Yu, Z., Elliott, E.M., 2017. Novel method for nitrogen isotopic analysis of soil-emitted nitric oxide. Environ. Sci. Technol. 51, 6268–6278. https://doi.org/10.1021/acs.est.7b00592.
Zhang, Y., Liu, J., Mu, Y., Pei, S., Lun, X., Chai, F., 2011. Emissions of nitrous oxide, nitrogen oxides and ammonia from a maize field in the North China Plain. Atmos. Environ. 45, 2956–2961. https://doi.org/10.1016/j.atmosenv.2010.10.052.
Zhou, X., Gao, H., He, Y., Huang, G., Bertman, S.B., Civerolo, K., Schwab, J., 2003. Nitric acid photolysis on surfaces in low-NO_x environments: significant atmospheric implications. Geophys. Res. Lett. 30, 2217. https://doi.org/10.1029/2003GL018620.
Zong, Z., Wang, X., Tian, C., Chen, Y., Fang, Y., Zhang, F., Li, C., Sun, J., Li, J., Zhang, G., 2017. First assessment of NO_x sources at a regional background site in North China using isotopic analysis linked with modeling. Environ. Sci. Technol. 51, 5923–5931. https://doi.org/10.1021/acs.est.6b06316.